Available online at www.sciencedirect.com

ScienceDirect

Procedia Manufacturing 19 (2018) 74–81

Procedia MANUFACTURING

www.elsevier.com/locate/procedia

6th International Conference on Through-life Engineering Services, TESConf 2017, 7-8 November 2017, Bremen, Germany

Ball end milling of titanium TIG weld material and the effect of SiC addition – process forces and shape deviations

B. Denkena[a], A.Mücke[a]*, T. Schumacher[a], D. Langen[b], T. Grove[a], B. Bergmann[a], T. Hassel[b]

[a]*Institute of Production Engineering and Machine Tools (IFW), Leibniz Universität Hannover, An der Universität 2, 30823 Garbsen, Germany*
[b]*Institute of Materials Science, Leibniz Universität Hannover (IW), An der Universität 2, 30823 Garbsen, Germany*

Abstract

An increasing amount of blade integrated disks (Blisks) is used in turbine engines. These integrally milled components offer benefits regarding to their performance-to-weight ratio. However, in case of failure, partial replacement is not possible. The Blisk has to be replaced entirely or repaired using re-generative processes for increased sustainability. Usually, a welding process is applied for patch repair or to build up a worn tip. Afterwards, a re-contouring process such as milling is needed to restore the original shape. To determine the influence of the welding process on the process forces during subsequent ball end milling, TIG welds have been re-contoured. Moreover, to achieve grain refinement in the fusion zone and enhanced mechanical properties, SiC was added to the weld pool. Process forces during milling as well as workpiece deflections were measured. It is shown, that the welding process has a serious impact on forces and needs to be considered for a precise process planning.

Peer-review under responsibility of the scientific committee of the 6th International Conference on Through-life Engineering Services.

Keywords: Titanium, Milling, Welding, Repair

* Corresponding author. Tel.: +49-511-762-18270; fax: +49-511-762-5115.
E-mail address: mueke@ifw.uni-hannover.de

2351-9789
Peer-review under responsibility of the scientific committee of the 6th International Conference on Through-life Engineering Services.
10.1016/j.promfg.2018.01.011

1. Introduction

The repair of complex capital goods, for example an aircraft engine, is a demanding task. Not only is the interaction of production processes with the components functionality complicated but also the interaction between the regeneration processes themselves. A typical example is the repair of blade integrated disks (Blisks) made of titanium alloy, which offer benefits regarding to their performance-to-weight ratio. However, their integral design limits the reparability. In case of failure, tailored regeneration processes must be available to secure sustainability. Otherwise, the Blisk has to be replaced entirely [1, 2].

Fig. 1. Phases of repair

A typical repair process chain of blades consists of four phases, namely pre-treatment, material deposit, re-contouring and post-treatment as depicted in Fig. 1 [1, 3, 4]. During pre-treatment, the part has to be prepared for the subsequent material deposit. Depending on the repair type (blend-, crack- or patch-repair), cleaning and/or machining processes are applied. For the material deposit, welding or brazing processes are typically used. In this paper, tungsten inert gas (TIG) welding is considered. It is commonly used for welding of titanium and titanium alloys. After the material deposit, the excess material has to be removed. The removal is done via grinding or cutting. For blisk-repair, 5-axis ball end milling is often used to restore the complex shape while facing a limited accessibility because of the adjacent blades [1, 4, 5]. Afterwards, post-treatment processes such as shot peening can be used to enhance surface integrity.

To ensure adequate functional and mechanical properties of the repaired components, the local alterations induced by the welding process must be considered during re-contouring. The properties of the welded joint differ from those of the base material (BM) and strongly depend on the grain size and microstructure of the welded seam [6, 7]. In the case of TIG welding, typically coarse, columnar grains are formed within the heat affected zone (HAZ) and the fusion zone (FZ). High cooling rates cause the formation of a Widmanstätten or a martensitic α‘ type of microstructure within the FZ. This kind of microstructure generally shows increased tensile strength accompanied by decreased ductility [8]. Following the theory of Hall-Petch-strengthening, grain-refinement in the FZ can be expected to improve the mechanical properties [9].

Today, only limited knowledge exists regarding repair and the interaction of the previously described processes. Thus, this paper contributes to the interaction between the TIG welding and subsequent 5-axis ball end milling process. In particular, TIG welds have been re-contoured to determine the influence of the welding process on the process forces during subsequent ball end milling. To investigate the influence of the microstructure, conventionally welded material as well as weld material with a fine grained FZ was re-contoured.

2. Methods

In order to characterize the influence of the TIG weld repair on the subsequent ball-end milling process, bead on plate welding was carried out on Ti-6Al-4V alloy substrates. These substrates were in the mill annealed condition according to AMS 4911. To investigate the cutting forces, rectangular samples with a size of 98 mm x 83 mm x 10 mm (type 1) were prepared. Moreover, to simulate possible shape deviations during application of the repair processes to real turbine blades, samples with a size of 110 mm x 45 mm x 5 mm (type 2) were machined. A 0.5 mm deep and 5 mm wide welding groove was milled in the samples along their longitudinal axis. These grooves were filled by one pass of TIG welding with Ti-6Al-4V welding wire of 1.0 mm in diameter. The chemical composition of the substrate and filler wire is shown in Table 1. In a first series, both sample types were conventionally welded. In order to investigate the influence of the formed microstructure, in particular the grain size within the FZ, SiC powder was added to the weld pool in a second series. A SiC suspension, containing acetone and SiC particles of 2 µm average size, was sprayed on the specimens to ensure a homogeneous distribution. Acetone was selected as the diluting agent given that it evaporates rapidly after spraying, leaving only the SiC particles on the groove’s surface. This method proved successful in that the SiC powder was sufficiently adhered to the surface resisting the shielding gas flow. A layer of 1.77 mg/mm SiC was measured on the groove’s surface prior to welding. The welding process was executed in a shielding gas chamber which sustained a protective argon gas atmosphere (O_2 content < 10 ppm).

Table 1. Chemical composition of substrate and filler wire.

Ti-6Al-4V in wt.-%	Substrate type 1	Substrate type 2	Filler wire
Al	6.32	6.15	6.05
V	3.94	3.80	4.1
O	0.16	0.12	0.18
Fe	0.17	0.12	0.18
C	0.007	0.013	0.08
N	0.001	0.002	0.03
H	0.004	0.006	0.015
Ti	bal.	bal.	bal.

For both series, an EWM Tetrix 350 AC/DC Plasma welding source was used. Table 2 shows the selected welding parameter sets for both sample types.

Table 2. Parameters of TIG welding processes

	Bead on plate type 1	Bead on plate type 2
Current, A	80	70
Shielding gas flow (Argon), l/min	4	4
Standoff distance, mm	3	3
Travel speed, mm/min	100	100
Wire feed, m/min	0.35	0.35

For optical microscopy, the samples were polished and then etched using Kroll's reagent. The morphological characteristics and changes of microstructure and grain size were evaluated. To measure the chemical composition of the weld material, a scanning electron microscope (SEM) Zeiss SUPRA 55 VP equipped with a Bruker EDX-Detector was used. Additionally, microhardness tests of the BM, FZ, and HAZ cross-sections were done using a Ness Q10 A+ Vickers apparatus with a 9.8 N load.

The milling experiments were carried out on a 5-axis machine tool featuring an electromagnetically guided z-axis. This machine tool is a prototype built by the Institute of Production Engineering and Machine Tools. For more information, one can refer to [10]. Cutting forces were estimated using the control output of the electromagnetic guide. Additionally, a dynamometer (Kistler 9257B) and a charge meter (Kistler 5015a) were applied to measure the cutting forces directly at the specimen. The signals of the dynamometer were captured at a sample rate of 20 kHz using the control hardware of the electromagnetic guide (Beckhoff I-PC, EtherCAT bus). For the cantilevered specimens, the workpiece deflection is measured by a Laser triangulation sensor (Keyence LKH-052) at a sample rate of 20 kHz. The length from the clamping device to the free edge of the cantilevered specimen measures 78 mm. The first Eigen frequency of the setup has been determined experimentally to approx. 570 Hz. The slot milling was performed measuring 25 mm from the top edge and 53 mm from the clamping device, respectively. This results in an analytically calculated static stiffness of approx. k_{stat} = 920 N/mm. The static stiffness is typical for re-contouring scenarios of blades from titanium.

In order to avoid influences from changing weld seam geometries or welding distortions on the cutting forces, all specimens were face milled by a shallow cut of 0.1 mm depth. The experimental cuts were then executed with a Seco JH970100 ball end mill (diameter D = 10 mm, flutes z = 2) with a depth of cut a_p = 0.3 mm. Thus, the tool cuts pure weld material when entering weld seam. Since the tool paths were transverse to the welding seam, every cut starts in the base material and then enters the HAZ and the FZ. The process parameters have been chosen according to typical finishing operations. A feed rate of f_z = 0.05 mm, a lead angle of $\lambda = 15°$ and a sharp tool (cutting edge rounding $r_\beta \sim 4$ µm) guarantee a high quality surface. The process parameters are summarized in Table 3.

Table 3. Parameters of 5-axis ball end milling process

	Bead on plate type 1 & 2
Cutting speed v_c, m/min	40
Feed per tooth f_z, mm	0.05
Depth of cut a_p, mm	0.3
Tool angle λ / τ, degrees °	15 / 0
Cutting edge radius r_β, µm	4

3. Results

A cross-section of a conventionally bead on plate welded sample without SiC addition is shown in Fig. 2 (1). Here, prior β-grains with an average size of 520 µm are observed within the FZ. However, towards the middle of the welded seam, grains of approximately 1 mm in length are seen.

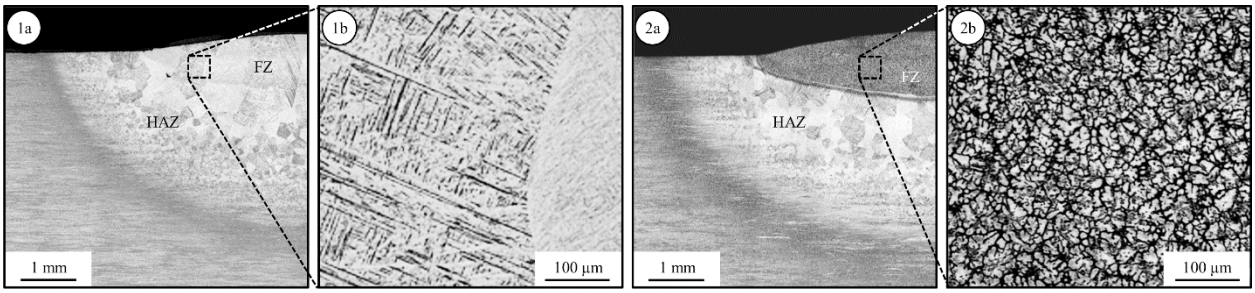

Fig. 2. Macro- (1a) and micrograph (1b) of a bead on plate weldment in cross sectional view, TIG welded without SiC addition. Macro- (2a) and micrograph (2b) of a bead on plate weldment in cross sectional view TIG welded with SiC addition, 3.3 wt-% Si.

A martensitic α' type of microstructure is seen among the prior β-grains. A distinct boundary between the FZ and the HAZ could not be identified. Nevertheless, in the HAZ, a grain size gradient can be observed with small grains staring at the substrate and bigger, coarser grains towards the transition to the FZ.

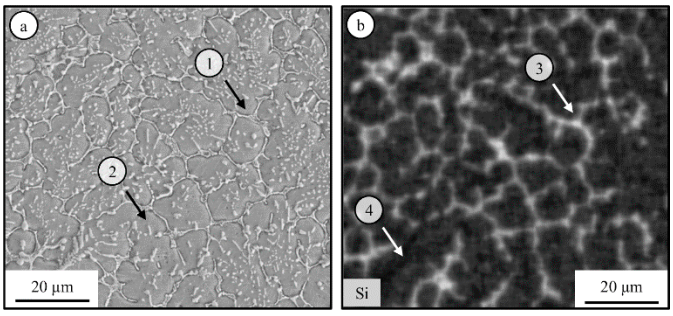

Fig. 3. (a) SE-image and (b) EDX silicon-distribution-map of welded specimen with SiC addition (3.3 wt.-% Si), with (1) prior β-grain boundaries and (2) titanium carbide particles. (3) enhanced Si content at the prior β-grain boundaries and (4) Si content below the detection limit near the titanium carbide particles.

Figure 2 (2) shows a cross-section of a TIG welded sample with SiC addition. In this case, a distinct boundary between the FZ und the HAZ is clearly observable. In the FZ, a homogeneous distribution of fine β-grains (22 µm average size) can be seen. The HAZ of SiC enhanced sample does not differ from the conventionally welded sample (cf. Fig. 2 (1)). The average silicon content in the FZ was measured to be 3.3 wt. %.

In Fig. 3, a secondary electron (SE) image (a) and an EDX silicon-distribution-map (b) of the FZ welded with SiC addition are shown. Areas with high Si-content appear bright in the EDX mapping and correspond with the boundaries of prior β-grains. Within the prior β-grains, titanium carbide particles were identified on the entire length of the FZ (Fig. 3, (2)). No silicon carbides or silicon-intermetallic bonds were found in the FZ.

The microhardness profile (HV1) of a conventionally welded specimen (left) as well as profile of SiC enhanced specimen (right) are depicted in Fig. 4. The highest hardness values were measured in the FZ, with a maximum of 384 HV1 for the conventional specimen and 479 HV1 for the SiC enhanced specimen. Both microhardness profiles have no gradient for the entire cross-section of the FZ and only a small gradient within the HAZ. However, for the SiC enhanced specimen, a rapid hardness decrease at the boundary between the FZ and HAZ is evident. The measured hardness values of the HAZ for the conventionally TIG welded sample ranged between 344 HV1 to 367 HV1 while those of the SiC enhanced sample ranged between 330 HV1 to 385 HV1. At the BM the measured microhardness was 318 HV1 (SD 3.01) for both specimens.

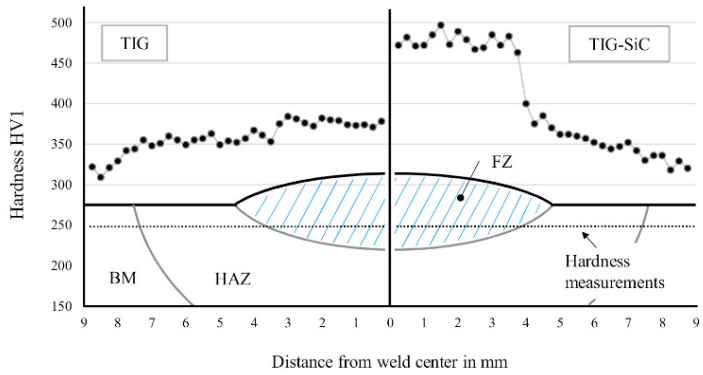

Fig. 4. Microhardness of a TIG welded specimen (left) and a TIG welded specimen with SiC addition (right), 3.3 wt.-% Si.

In Fig. 5 (a), process forces during milling of the TIG welded specimen (type 1) are shown. Therefore, the static process forces $F_{i,stat}$ as well as the maximum force $F_{i,max}$ were determined. They have been calculated using digital filtering ($F_{i,stat}$) as well as analytic envelopes ($F_{i,max}$). They are shown in the workpiece coordinate system consisting of passive force F_p, feed force F_f and feed normal force F_{fn}.

Regarding the process forces in Fig. 5 (a), the process forces remain almost unchanged. There is no change visible when entering the HAZ. Only a slight increase of the passive force F_p can be detected in the FZ. The static passive force $F_{p,stat}$ raises about 2 N and 10 %, respectively. The maximum passive Force $F_{p,max}$ is increased about 8 N and accordingly 20 %. The process forces for re-contouring the TIG welded specimen with SiC addition (type 1) are depicted in Fig. 5 (b). Again, there is no change visible when entering the HAZ. A significant increase of all process forces can be observed when entering the fusion zone FZ. The passive force F_p is almost doubled. The max. feed force $F_{f,max}$ as well as the max. feed normal force $F_{fn,max}$ are increased by 7 N (20 %) and 12 N (18 %), respectively.

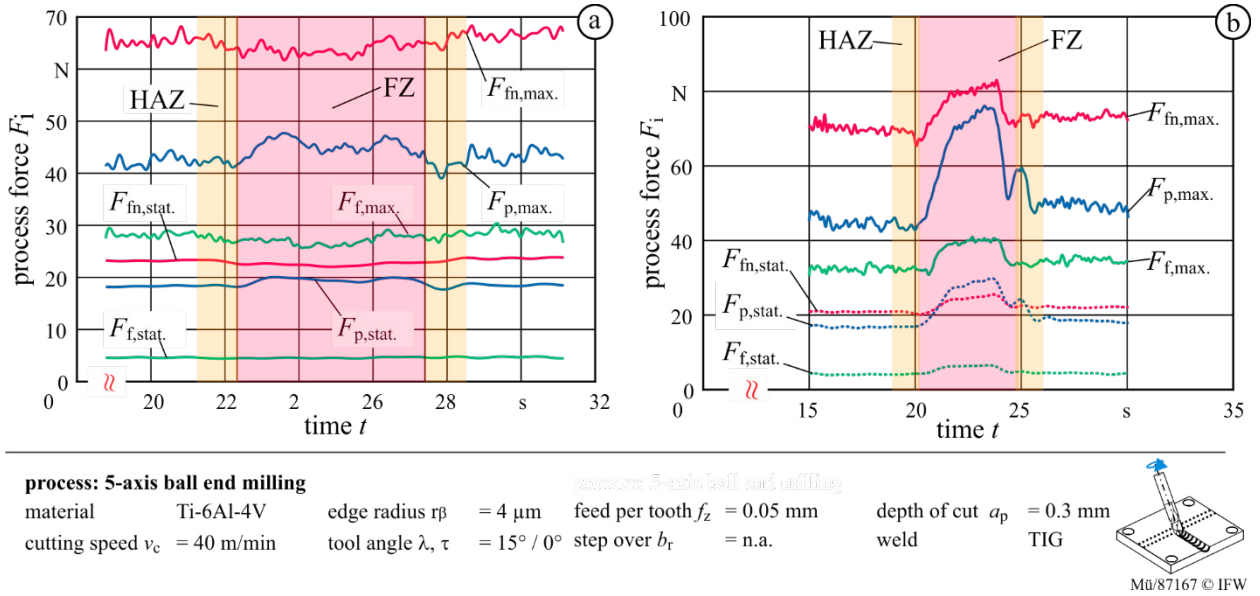

Fig. 5. Static and maximum process forces during slot milling of rigid TIG welded specimen (a) and TIG welded specimen with SIC addition (b).

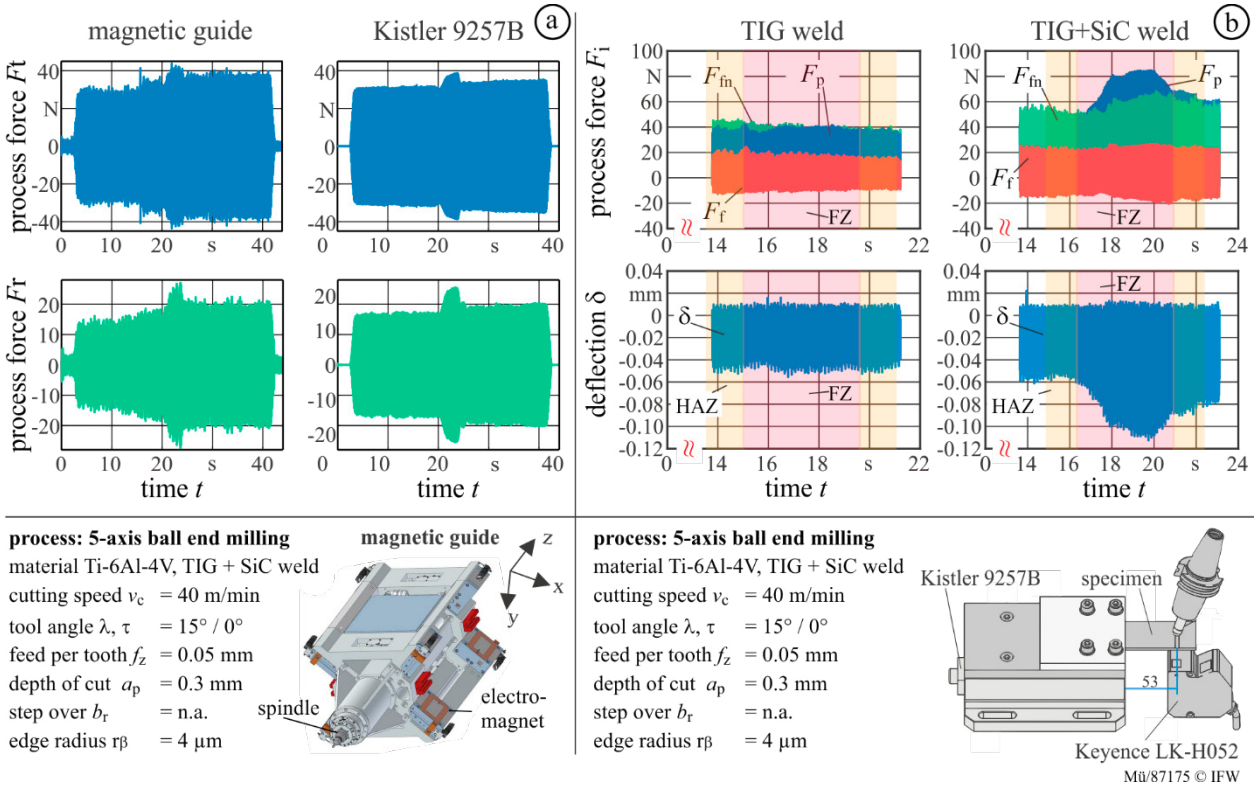

Fig. 6. Comparison of tangential force F_t and radial force F_r measured by the magnetic guide and dynamometer type Kistler 9257B (a). Process forces and workpiece deflection for slot milling a cantilever beam at k_{stat} = 920 N/mm (b).

On the tool side, the magnetic guide detects radial and tangential process forces. Figure 6 (a) shows these forces for re-contouring of the TIG welded specimen with SiC addition (type 1). Reference forces were calculated from dynamometer measurements by transformation of coordinates. Both signals were filtered using a bandpass with lower and upper cutoff frequencies of 25 Hz and 50 Hz, respectively. Thus, disturbance forces on the magnetic guide (e.g. passive forces of the linear direct drives or drag forces from cables) and natural frequencies of the machine tool are suppressed.

As depicted in Fig. 6 (a), the forces measured by the magnetic guide are in good agreement with the reference forces from the dynamometer. This underlines the capabilities of the magnetic guide for process control.

To analyze the effect of increased process forces for a typical re-contouring scenario, flexible specimens were milled (type 2). The process forces as well as the workpiece deflection in the direction of passive force F_p are shown in Fig. 6 (b). The process forces and deflection for the conventional TIG welded specimen remain constant when entering the different zones BM, HAZ and FZ. A constant deflection of approx. 0.05 mm has been measured, which leads directly to shape errors. The desired depth of cut a_p has not been reached.

When milling the TIG+SiC welded specimen, the process forces show the same characteristics as depicted in Fig. 6 (b). If the tool enters the fusion zone FZ, the passive force F_p and thus the deflection δ in the same direction is raised significantly. The maximum deflection δ exceeds 0.1 mm.

4. Discussion

The observed microstructural changes of the conventional TIG welded specimen result in lower ductility and poor mechanical properties similar to the casted state of Ti-6Al-4V. This can be credited to the gradual increase of prior β-grain sizes and the presence of martensitic α' microstructure as seen in Fig. 2 (1) [11]. The present investigation demonstrates that these microstructural changes, and therefore changes in mechanical properties, can be controlled by SiC addition. SiC prevents the gradual growth of β-grains, supporting a homogenous distribution of α-titanium and intergranular β-phases in the FZ. In particular, this inhibits the directional growth of partly molten β-grains from the HAZ into the FZ, resulting in the observed, distinct borderline (cf. Fig. 2 (2)). In the FZ a significant amount of titanium carbides but no silicon carbides were detected. Therefore, it can be concluded that the SiC particles are dissociated during welding. Thus, heterogeneous nucleation induced by the added SiC particles is not solely accountable for the produced grain refinement. Elevated Si-content near the grain boundaries suggests that a Si-rich layer was formed at the solid-liquid-interface during solidification. The high Si content leads to a local decrease of the liquidus temperature below the melt temperature at that position, a process known as constitutional supercooling which also leads to grain refinement [12, 13].

Both, the presence of the titanium carbide particles and the resulting grain refinement, can be responsible for the observed microhardness increase of about 113 HV1 in the FZ of the SiC enhanced TIG welded samples (Fig. 4).

The influence of the SiC addition on the process forces during subsequent re-contouring is significant. Without the SiC addition, the hardness of the weld remains almost unchanged if compared to the base material. Only a slight increase is visible in the passive force F_p during milling. However, due to the grain refinement and the allocation of titanium carbides within the FZ of the SiC-enhanced specimens, the process forces are increased significantly. Especially the max. passive force $F_{p,max}$ is affected. The measurements of the magnetic guide show good consistency with the dynamometer measurements and relatively small changes in force can be detected.

The effects could also be shown when milling the vibration prone parts. The higher resulting deflection leads to the conclusion, that either additional clamping systems are required or the process parameters have to be reduced when re-contouring flexible TIG+SiC welded parts with a conventional machine tool. As an alternative, a magnetic guide can be used as a sensor and actuator. It allows the reduction of shape errors by deflection compensation [14]. Future research will apply the methods from [14] to maintain high productivity despite different weld characteristics.

5. Conclusion & Outlook

To extend the knowledge regarding repair and especially re-contouring of turbine components, the influence of the TIG welding process on the process forces during subsequent ball-end milling has been investigated. First, bead on

plate welding was carried out on Ti-6Al-4V alloy substrate specimens using a conventional TIG process. To achieve grain refinement and enhanced material properties in the fusion zone, SiC was added to the weld pool.

The welds were analyzed regarding their microstructure and hardness. It could be shown that the SiC addition leads to a significant grain refinement and higher hardness. When re-contouring the different specimens, the TIG+SiC welds showed increased process forces and a twice as high deflection. For a precise process planning, this has to be taken into account. Thus, a reduction of process parameters or additional clamping systems may be required. Future research will deal with the amount of SiC powder needed to achieve specific material properties. Furthermore, the weld characteristics will be included in a material removal simulation to predict process forces for an efficient process planning of re-contouring tasks.

Additionally, the use of artificial intelligence to model disturbance forces on the magnetic guide will improve the measurement accuracy. This allows a precise detection of different workpiece conditions, which enables the optimization across the re-generative processes.

Acknowledgements

The authors kindly thank the German Research Foundation (DFG) for the financial support of the Collaborative Research Center (SFB) 871 “Regeneration of Complex Capital Goods” which provides the opportunity of their collaboration in the research projects B2 “Dexterous Regeneration Cell”, B6 “Arc welding processes for repair of high-performance titanium-alloy components” and C1 “Simulation Based Planning of Recontouring Metal Cutting Processes”.

References

[1] Eberlein A. Phases of high-tech repair implementation. 18th International Symposium on Airbreathing Engines (ISABE) Beijing 2007.

[2] Kelbassa I, Gasser, A, Backes G, Keutgen S, Kreutz E-W, Pirch N. Repair and (Re)conditioning of Compressor and Turbine Blades by CO_2 and Nd:YAG Laser Radiation. Schriften des Forschungszentrums Jülich. Energy Technology 2002;21:751-758.

[3] Bremer C. Automated Repair and Overhaul System for Aero Turbine Engine Components (AROSATEC). Tech. Rep. BCT/Alround/ISQ/Metris/MTU/Sifco/Skytek 2006.

[4] Yilmaz O, Gindy N, Gao J. A Repair and Overhaul Methodology for Aeroengine Components. Robotics and Computer-Integrated Manufacturing 2010;26/2:190-201.

[5] Gao J, Chen X, Yilmaz O, Gindy N. An Integrated Adaptive Repair Solution for Complex Aerospace Components Through Geometry Reconstruction. Int J of Advanced Manufacturing Technology 2008;36/11-12:1170-1179.

[6] Mehdi B, Badji R, Ji V, Allili, B, Bradai, D, Deschaux-Beaume, F, Soulié F. Microstructure and residual stresses in Ti-6Al-4V alloy pulsed and unpulsed TIG welds. J Mater Process Technol 2016;231:441-448.

[7] Balasubramanian M, Jayabalan V, Balasubramanian V. Effect of microstructure on impact toughness of pulsed current GTA welded α-β titanium alloy. Mater Lett 2008;62:1102-1106.

[8] Balasubramanian TS, Balakrishnan M, Balasubramanian V, Muthu Manickam MA. Effect of welding processes on joint characteristics of Ti-6Al-4V alloy. Sci Technol Weld Joining 2013;16:702-708.

[9] Balasubramanian V, Jayabalan V, Balasubramanian M. Effect of current pulsing on tensile properties of titanium alloy. Mater Des 2008;29:1459-1466.

[10] Flöter F, Denkena B. Analysis of chatter vibration and tool deflection in milling with a novel active machine tool guide. Applied Mechanics and Materials 2015;794:331-338.

[11] Kabir ASH, Cao X, Gholipour J, Wanjara P, Cuddy J, Birur A, Medraj M. Effect of Postweld Heat Treatment on Microstructure, Hardness, and Tensile Properties of Laser-Welded Ti-6Al-4V. Metall Mater Trans A 2012;43:4171-4184.

[12] Kou S. Welding metallurgy. 2nd ed. New Jersey: Wiley-Interscience, 2003.

[13] Bermingham M, McDonald S, Dargusch MS, StJohn D. Latest Developments in Understanding the Grain Refinement of Cast Titanium. Mater Sci Forum 2009:315-318.

[14] Flöter, F. Potentiale einer elektromagnetischen Führung in Fräsmaschinen und ihr Nutzen für die Reparaturbearbeitung. Dr.-Ing. Dissertation Universität Hannover. PZH-Verlag 2017.